

# Atomic Force Microscopy Study of Layered MnPS<sub>3</sub> and Its Intercalation Compounds

Isabelle Lagadic, René Clément,\* and Olivier Kahn

Laboratoire de Chimie Inorganique, C.N.R.S. U.R.A. No. 420, Université de Paris-Sud,  
91405 Orsay Cedex, France

Jingqing Ren and Myung-Hwan Whangbo\*

Department of Chemistry, North Carolina State University,  
Raleigh, North Carolina 27695-8204

Received March 11, 1994. Revised Manuscript Received August 5, 1994<sup>®</sup>

The layered phase MnPS<sub>3</sub> and its intercalation compounds Mn<sub>1-x</sub>PS<sub>3</sub>G<sub>2x</sub> (G = potassium, pyridinium, and tetramethylammonium cations) were examined by atomic force microscopy (AFM). These compounds have layers made up of close packed P<sub>2</sub>S<sub>6</sub><sup>4-</sup> ions with their P-P bonds perpendicular to the layer plane. The atomic-resolution AFM images observed for these compounds are characterized by two hexagonal patterns, i.e., the regular and superstructure patterns of the ~3.5 and ~6.5 Å periods, respectively. This finding was interpreted by calculating the total electron density plots of MnPS<sub>3</sub> layers in which the P<sub>2</sub>S<sub>6</sub><sup>4-</sup> ions tilt slightly from their perpendicular arrangement. The regular pattern is explained by the surface sulfur atoms of the topmost layer and the superstructure by the pattern of the protruded surface sulfur atoms that results when the P<sub>2</sub>S<sub>6</sub><sup>4-</sup> ions tilt slightly. The tilting of the P<sub>2</sub>S<sub>6</sub><sup>4-</sup> ions may be caused by the guest species present between the layers.

## Introduction

Since the discovery of scanning tunneling microscopy (STM)<sup>1</sup> and atomic force microscopy (AFM),<sup>2–5</sup> the surfaces of various layered compounds have been characterized.<sup>6–11</sup> Some of these studies exhibit striking features such as charge density waves.<sup>12–16</sup> In contrast, intercalation compounds have not been extensively studied by STM and AFM,<sup>17–22</sup> which is due probably to the air sensitivity and poor crystallinity of most

intercalation compounds. Investigation of intercalation compounds on the atomic scale is potentially important for two reasons. First, intercalation allows one to chemically modify materials with planar and well-characterized surface in a controlled way. STM and AFM studies of these materials may help interpret the resulting images and hence develop the analytical capabilities of these techniques. Second, intercalation chemistry may provide a natural way to organize surface architecture of molecules that can be used as convenient workbenches for a future “molecular electronics”.

Hexathiohypodiphosphates MPS<sub>3</sub>, where M is a transition metal in +2 oxidation state, are layered insulating materials<sup>23–25</sup> that are available as highly planar platelets. MPS<sub>3</sub> is intercalated by a variety of molecular species, and the resulting intercalation compounds are air stable over very long periods.<sup>26,27</sup> A wide range of M<sub>1-x</sub>PS<sub>3</sub>G<sub>2x</sub> intercalates, where G refers to a monocation, can be synthesized via a cation-exchange process in which the electrical charge of entering cationic guest species G<sup>+</sup> is counterbalanced by the loss of some intralayer M<sup>2+</sup> cations.<sup>26,27</sup> This chemistry has been extensively developed over the past 10 years, as many

\* To whom correspondence should be addressed.

<sup>®</sup> Abstract published in *Advance ACS Abstracts*, September 15, 1994.

- (1) Binnig, G.; Rohrer, H. *Helv. Phys. Acta* **1982**, *55*, 726.
- (2) Binnig, G.; Quate, C. F.; Gerber, Ch. *Phys. Rev. Lett.* **1986**, *56*, 930.
- (3) Binnig, G.; Gerber, Ch.; Stoll, E.; Albrecht, T. R.; Quate, C. F. *Europhys. Lett.* **1987**, *3*, 1281.
- (4) Albrecht, T. R.; Quate, C. F. *J. Appl. Phys.* **1987**, *62*, 2599.
- (5) Shindo, H.; Kaise, M.; Kondoh, H.; Nishihara, C.; Hayakawa, H.; Ono, S.; Nozoye, H. *J. Chem. Soc., Chem. Commun.* **1991**, 1097.
- (6) Frommer, J. *Angew. Chem., Int. Ed. Engl.* **1992**, *31*, 1298.
- (7) Miller, R. G.; Bryant, P. J. *J. Vac. Sci. Technol. A* **1989**, *7*, 2879.
- (8) Coleman, R.; Giambattista, R.; Hansma, P.; Johnson, A.; McNairy, W.; Slough, S. C. *Adv. Phys.* **1988**, *37*, 559.
- (9) Lieber, C. M.; Wu, X. L. *Acc. Chem. Res.* **1991**, *24*, 170 and references therein.
- (10) Parkinson, B. A. *J. Am. Chem. Soc.* **1990**, *112*, 7498.
- (11) Delawski, E.; Parkinson, B. A. *J. Am. Chem. Soc.* **1992**, *114*, 1661.
- (12) Garnaes, J.; Gould, S. A. C.; Hansma, P. K.; Coleman, R. V. *J. Vac. Sci. Technol. B* **1991**, *9*, 1032.
- (13) Meyer, E.; Wiesendanger, R.; Anselmetti, D.; Hidber, H. R.; Güntherodt, H. J.; Levy, F.; Berger, H. *J. Vac. Sci. Technol. A* **1990**, *8*, 495.
- (14) Barrett, R. C.; Nogami, J.; Quate, C. F. *Appl. Phys. Lett.* **1990**, *57*, 992.
- (15) Wu, X. L.; Lieber, C. M. *Science* **1989**, *243*, 1703.
- (16) Chen, H.; Wu, X. L.; Lieber, C. M. *J. Am. Chem. Soc.* **1990**, *112*, 3326.
- (17) Lang, H. P.; Wiesendanger, R.; Thommen-Geiser, V.; Güntherodt, H. *J. Phys. Rev. B* **1992**, *45*, 1829.
- (18) Kelty, S. P.; Lieber, C. M. *Phys. Rev. B* **1989**, *40*, 5856.
- (19) Biensan, P.; Roux, J. C.; Saadaoui, H.; Flandrois, S. *J. Microanal. Microstruct.* **1990**, *1*, 103; **1991**, *2*, 465.
- (20) Shindo, H.; Nozoye, H. *Jpn. J. Appl. Phys.* **1993**, *32*, 2950.

(21) Pappas, R. A.; Hunt, E. R.; Ulloa, S. E. *Ultramicroscopy* **1992**, *42*–*44*, 679.

(22) Anselmetti, D.; Wiesendanger, R.; Güntherodt, H.-J. *Phys. Rev. B* **1989**, *39*, 11135.

(23) (a) Klingen, W.; Ott, R.; Hahn, H. *Z. Anorg. Allg. Chem.* **1973**, *396*, 271. (b) Klingen, W.; Eulenberger, G.; Hahn, H. *Z. Anorg. Allg. Chem.* **1973**, *401*, 97.

(24) O'Hare, D. In *Inorganic Materials*; Bruce, D. W., O'Hare, D., Eds.; John Wiley: Chichester, 1992; Chapter 4.

(25) Jacobson, A. In *Solid State Chemistry Compounds*; Cheetham, A. K., Day, P., Eds.; Oxford Science Publications: Clarendon Press, Oxford, 1992; p 204.

(26) Clément, R. *J. Chem. Soc., Chem. Commun.* **1980**, 647.

(27) Clément, R.; Garnier, O.; Jegoudez, J. *Inorg. Chem.* **1986**, *25*, 1404.

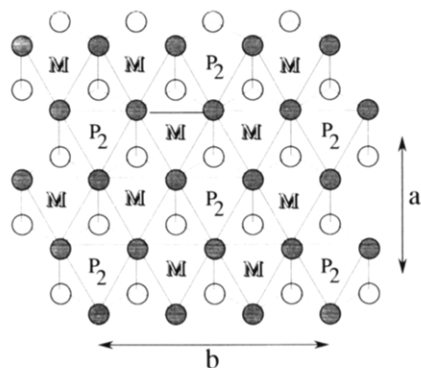


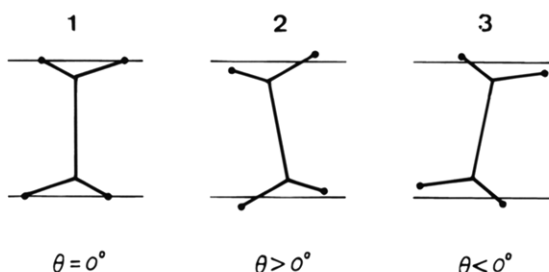
**Figure 1.** Schematic top view of a single MnPS<sub>3</sub> layer, which consists of close-packed P<sub>2</sub>S<sub>6</sub><sup>4-</sup> ions. The Mn<sup>2+</sup> ions are located in the octahedral sites of sulfur atoms (represented by circles) generated by every three adjacent P<sub>2</sub>S<sub>6</sub><sup>4-</sup> ions. The *a* and *b* axes of the monoclinic unit cell are shown (*a* = 6.077 Å, *b* = 10.524 Å).

of these intercalates have magnetic, electrical, and nonlinear optical properties very different from those of the pure host lattice.<sup>28,29</sup>

In the present work, we report AFM studies of MnPS<sub>3</sub> and intercalation compounds Mn<sub>1-x</sub>PS<sub>3</sub>G<sub>2x</sub> (G = potassium, pyridinium, and tetramethylammonium ions). All these materials are insulating, which precludes their STM characterization.

### Structures of MnPS<sub>3</sub> and Its Mn<sub>1-x</sub>PS<sub>3</sub>G<sub>2x</sub> Intercalates

For our later discussion of the AFM images of MnPS<sub>3</sub> phase and Mn<sub>1-x</sub>PS<sub>3</sub>G<sub>2x</sub> intercalates, it is necessary to describe their structures. An MnPS<sub>3</sub> layer is made up of Mn<sup>2+</sup> and P<sub>2</sub>S<sub>6</sub><sup>4-</sup> ions as schematically shown in Figure 1. Two PS<sub>3</sub> pyramids of a P<sub>2</sub>S<sub>6</sub><sup>4-</sup> ion are joined by a P-P bond and arranged in a staggered conformation as in staggered ethane C<sub>2</sub>H<sub>6</sub>. In each MnPS<sub>3</sub> layer, the P<sub>2</sub>S<sub>6</sub><sup>4-</sup> ions have their P-P bonds perpendicular to the layer (see 1), the Mn<sup>2+</sup> ions are located in the



octahedral sites of sulfur atoms formed by three adjacent P<sub>2</sub>S<sub>6</sub><sup>4-</sup> ions, and the surfaces have hexagonally arranged sulfur atoms (Figure 1). The shortest Mn-Mn or S-S distance is 3.508 Å, and two adjacent P<sub>2</sub>S<sub>6</sub><sup>4-</sup> ions of an MnPS<sub>3</sub> layer are separated by 6.077 Å.

Although detailed refined structures of the Mn<sub>1-x</sub>PS<sub>3</sub>G<sub>2x</sub> intercalates are not available, important structural aspects are known. The intercalates are quite well crystallized, in the sense that they exhibit X-ray powder diffraction patterns with sharp reflections. Insertion of guest ions and departure of Mn<sup>2+</sup> ions occur spontaneously at room temperature within a few minutes,

revealing a rather weak bonding between Mn<sup>2+</sup> and P<sub>2</sub>S<sub>6</sub><sup>4-</sup> ions, which is favorable for facile lattice deformations. The Mn<sup>2+</sup> departure results in the occurrence of vacancies within the layers, and it has been shown recently that these vacancies order to form superlattices,<sup>30,31</sup> involving in particular tripling of the *a* axis of the monoclinic unit cell. Thus, a symmetry lowering accompanies the intercalation. Recent infrared and Raman studies have shown that the center of symmetry in pristine MnPS<sub>3</sub> is removed upon intercalating pyridine.<sup>32</sup> Analysis of the luminescence spectra of intercalated rare-earth cations show strong Stark effects due to a very low local symmetry.<sup>33</sup> The recent finding of strong quadratic nonlinear optical properties of MPS<sub>3</sub>-stilbazolium intercalates<sup>29</sup> implies a noncentrosymmetrical arrangement of the organic chromophores. Therefore it is interesting to see if AFM can be used to characterize the symmetry lowering in molecular scale.

### Experimental Section

Pure MnPS<sub>3</sub> was synthesized as already described.<sup>23</sup> Monocrystalline platelets (about 4 × 4 × 0.05 mm<sup>3</sup>) were grown from the vapor phase by heating a stoichiometric mixture of the elements at 750 to 780 °C in sealed evacuated quartz ampules. Intercalation of potassium (K<sup>+</sup>), tetramethylammonium (Me<sub>4</sub>N<sup>+</sup>), and pyridinium (pyH<sup>+</sup>) ions was performed by soaking MnPS<sub>3</sub> platelets into an excess of approximately 2 M aqueous solutions of KCl, Me<sub>4</sub>NCl, or pyHCl, respectively, for about 15 min.<sup>26,28</sup> The intercalated platelets were then rinsed with water and dried in air. The samples were finally glued on the sample holder and cleaved prior to examination.

Imaging the sample surface was carried out using a commercial AFM apparatus (Nanoscope II) with a contact mode (a 100 μm long cantilever of spring force constant of 0.58 N/m and a Si<sub>3</sub>N<sub>4</sub> tip). The force employed was about 2.5 × 10<sup>-8</sup> N. The surface of the crystal samples were scanned (10–20 lines/s) using the height mode, in which the force between the tip and the surface is kept constant. All images (400 × 400 pixels) were obtained in air at room temperature using a slight high- and low-pass filtering during the data acquisition (positions 4 and 1, respectively, in the Nanoscope software).

**Pure MnPS<sub>3</sub>.** Scanning of a number of pure MnPS<sub>3</sub> samples reveals two types of images, which we referred to as the regular and superstructure patterns in the following. An unfiltered image of the regular pattern is shown in Figure 2a, which displays a hexagonal pattern of spots separated by ~3.5 Å.<sup>34</sup> The latter is the same as the S-S distance on the surface sulfur atom sheet of MnPS<sub>3</sub>.<sup>23,35</sup> The two-dimensional (2D) power spectrum of the Fourier transform of this image (Figure 2b) shows only one repeating period and confirms a near-hexagonal symmetry. The observed height corrugation is about 1–2 Å, which is too large to be explained by variations in the total charge density. It is suggested that frictional forces operate with an atomic periodicity.<sup>14,35–38</sup> Images of the superstructure pattern are shown in Figure 3. A hexagonal pattern of spots can still be observed in direct space, but the

(30) Clément, R.; Lagadic, I.; Léautié, A.; Audiére, J. P.; Lomas, L. In *Chemical Physics of Intercalation II*; Bernier, P., Fisher, J. E., Roth, S., Solin, S. A., Eds.; NATO ASI Series B **1993**, 305, 315.

(31) Evans, J. *Thesis*, University of Oxford, U.K., 1993.

(32) Joy, P. A.; Vasudevan, S. *J. Am. Chem. Soc.* **1992**, 114, 7792.

(33) Clément, R.; Léautié, A.; Marney, K.; Francis, A. H. *J. Phys. Chem. Solids*, in press.

(34) The error of the measured distances is estimated to be ~10%, which is due to the thermal drift and other uncertainties.

(35) Meyer, E.; Heinzelman, H. In *Scanning Tunneling Microscopy II*; Wiesendanger, R., Güntherodt, H.-J., Eds.; Springer: Berlin, 1992; pp 99–149 and references therein.

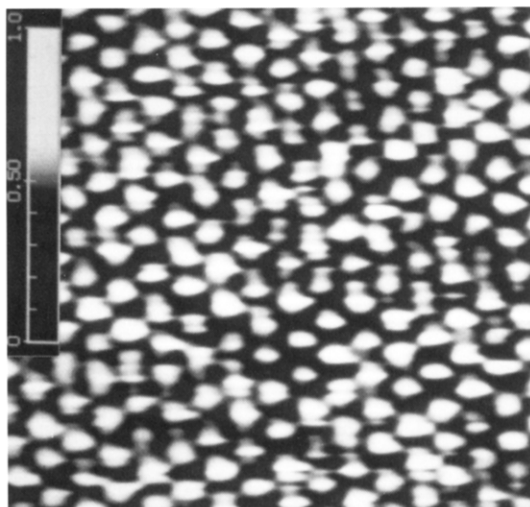
(36) Mate, C. M.; Mc Clelland, G. M.; Erlandsson, R.; Chiang, S. *Phys. Rev. Lett.* **1987**, 59, 1942.

(37) Erlandsson, R.; Hadzioannou, G.; Mate, C. M.; Mc Clelland, G. M.; Chiang, S. *J. Chem. Phys.* **1988**, 89, 5190.

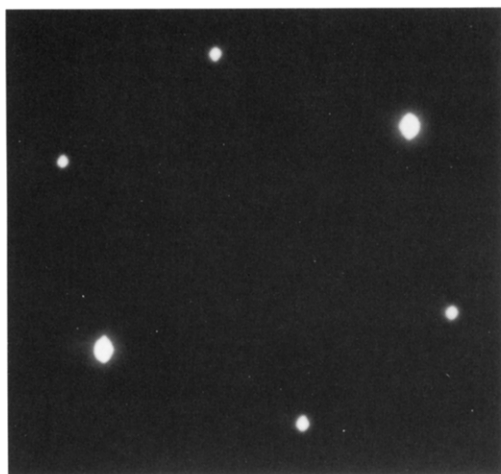
(38) Colchero, J.; Bielefeldt, H.; Ruf, A.; Hipp, M.; Marti, O.; Mlynk, J. *Phys. Status Solidi* **1992**, 131, 73.

(28) Clément, R.; Lomas, L.; Audiére, J. P. *Chem. Mater.* **1990**, 2, 641.

(29) Lacroix, P.; Clément, R.; Nakatani, K.; Zyss, J.; Ledoux, I. *Science* **1994**, 263, 658.



2a



2b

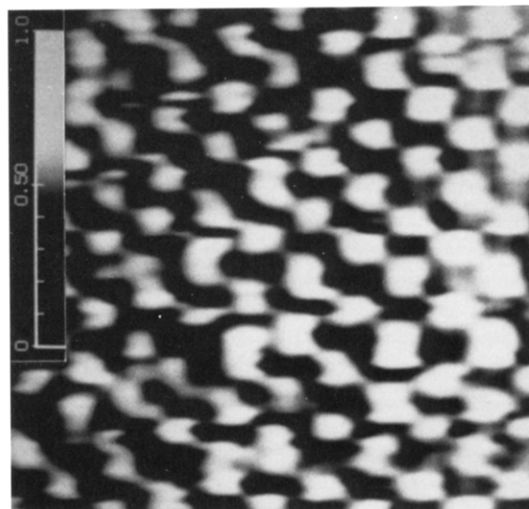
**Figure 2.** (a) Unfiltered AFM image (regular pattern) of  $\text{MnPS}_3$  (height mode,  $8 \times 8 \text{ nm}^2$  area). (b) 2D power spectrum of Figure 2a.

period of the superstructure ( $\sim 6.5 \text{ \AA}$ )<sup>34</sup> is about twice that of the regular pattern (i.e.,  $\sim 3.5 \text{ \AA}$ ).

For  $\text{MnPS}_3$ , images of both the regular and superstructure patterns are frequently recorded on a same sample in different areas, and sometimes both are observed even on a same scan. The unfiltered image of Figure 4a resembles that of Figure 2a, but its 2D power spectrum (Figure 4b) displays 12 spots grouped in two hexagons, the inner one being rotated by  $30^\circ$  with respect to the outer one. The outer peaks correspond to the regular pattern, and the inner ones to the superstructure. The occurrence of the two patterns is not obvious in the unfiltered image of Figure 4a but can be seen from an inverse Fourier transform based on the 12 intense peaks of the 2D power spectrum. For example, the bottom left corner of Figure 4c shows a superposition of the two patterns. The corrugation difference between the bright and dim spots is  $\sim 0.6 \text{ \AA}$ .

A series of scans show that 2D power spectra do not always possess two imbricated hexagons because two spots of the inner hexagon (corresponding to the superstructure pattern in real space) are often missing. Some areas of the images switch from the regular to the superstructure pattern, and vice versa, during scanning. This indicates a delicate dynamical modification of the surface.

**$\text{Mn}_{1-x}\text{PS}_3\text{G}_{2x}$  ( $\text{G} = \text{K, pyH, Me}_4\text{N}$ ) Intercalates.** Figure 5a shows an unfiltered image obtained for a platelet of  $\text{Mn}_{1-x}\text{PS}_3\text{K}_{2x}$ . The image appears somewhat noisy but has an atomic scale resolution, and its 2D power spectrum displays peaks made up of two imbricated hexagons (Figure 5b). These hexagons correspond to the regular pattern (outer one) and the superstructure pattern (inner one) already observed for



3a



3b

**Figure 3.** (a) Unfiltered AFM image (superstructure pattern) of  $\text{MnPS}_3$  (height mode,  $6 \times 6 \text{ nm}^2$  area). (b) 2D power spectrum of Figure 3a.

pure  $\text{MnPS}_3$ . The peaks of the inner hexagon are intense, and two peaks of the outer hexagon are weak or even missing in some cases. The inverse Fourier transform based on the twelve bright spots of the 2D power spectrum clearly shows a superposition of the two hexagonal patterns with different brightness (or, equivalently, heights; Figure 5c). The bright spots are separated by  $\sim 6.5 \text{ \AA}$ , and the dim ones by  $\sim 3.5 \text{ \AA}$ . These periods observed for  $\text{Mn}_{1-x}\text{PS}_3\text{K}_{2x}$  are the same as those found for pure  $\text{MnPS}_3$ , but the contrast between the bright and dim spots is more pronounced for the potassium intercalate. A similar image is obtained for many different samples of  $\text{Mn}_{1-x}\text{PS}_3\text{K}_{2x}$ , and the nature of the image does not change with time, in contrast to the case of pure  $\text{MnPS}_3$  samples. Images obtained for  $\text{Mn}_{1-x}\text{PS}_3(\text{pyH})_{2x}$  are very similar to those recorded for  $\text{Mn}_{1-x}\text{PS}_3\text{K}_{2x}$ . Images obtained for  $\text{Mn}_{1-x}\text{PS}_3(\text{Me}_4\text{N})_{2x}$  are shown in Figures 6a (unfiltered image), 6b (2D power spectrum), and 6c (filtered image). The image of  $\text{Mn}_{1-x}\text{PS}_3(\text{Me}_4\text{N})_{2x}$  (Figure 6c) has triangles of one dim and two bright spots (with the height difference of about  $0.8 \text{ \AA}$ ). This is different from the superstructure patterns of  $\text{MnPS}_3$ ,  $\text{Mn}_{1-x}\text{PS}_3\text{K}_{2x}$ , and  $\text{Mn}_{1-x}\text{PS}_3(\text{pyH})_{2x}$ , which have triangles of one bright and two dim spots.

## Discussion

It is important to examine how the regular and superstructure patterns of the AFM images can be explained. We first consider the superstructure pattern of the  $\sim 6.5 \text{ \AA}$  period observed for  $\text{Mn}_{1-x}\text{PS}_3\text{K}_{2x}$  (Figure

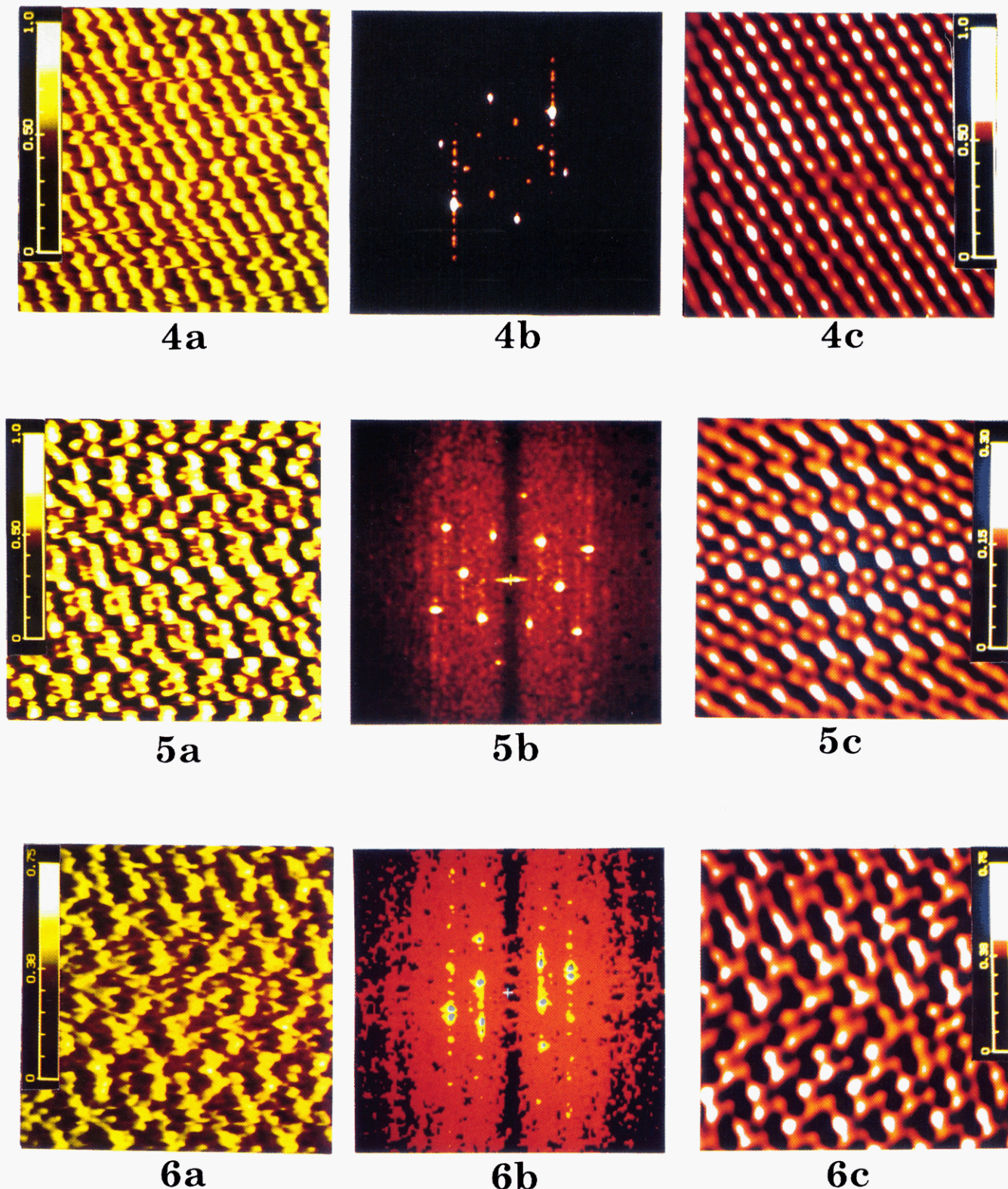


**Figure 4.** (a) Unfiltered AFM image of MnPS<sub>3</sub> possessing both the regular and superstructure patterns (height mode, 8 × 8 nm<sup>2</sup> area). (b) 2D power spectrum of Figure 4a, where 12 peaks form two imbricated hexagons. The other peaks arise from noise or instrumental effects. (c) Filtered image of MnPS<sub>3</sub> obtained by an inverse Fourier transform retaining only the twelve peaks of the two hexagons in Figure 4b. **Figure 5.** (a) Unfiltered AFM image of Mn<sub>1-x</sub>PS<sub>3</sub>K<sub>2x</sub> (height mode, 8 × 8 nm<sup>2</sup> area). (b) 2D power spectrum of Figure 5a, where 12 peaks form two imbricated hexagons. (c) Filtered image of Mn<sub>1-x</sub>PS<sub>3</sub>K<sub>2x</sub> obtained by an inverse Fourier transform retaining only the 12 peaks of the two hexagons in Figure 5b. **Figure 6.** (a) Unfiltered AFM image of Mn<sub>1-x</sub>PS<sub>3</sub>(Me<sub>4</sub>N)<sub>2x</sub> (height mode, 6 × 6 nm<sup>2</sup> area). (b) 2D power spectrum of Figure 6a, where eight bright peaks form an inner lozenge imbricated in a slightly distorted rectangle. (c) Filtered image of Mn<sub>1-x</sub>PS<sub>3</sub>(Me<sub>4</sub>N)<sub>2x</sub> obtained by an inverse Fourier transform retaining only the eight peaks of Figure 6b.

5c). One might speculate these spots to represent potassium cations sitting in an ordered way on top of the surface sulfur atoms, but this possibility is ruled out because a similar image is also observed for MnPS<sub>3</sub>

and Mn<sub>1-x</sub>PS<sub>3</sub>(pyH)<sub>2x</sub>. An alternative possibility is that all (bright and dim) spots of Figure 5c represent the surface sulfur atoms, with certain sulfur atoms protruded in a periodic way to make the superstructure

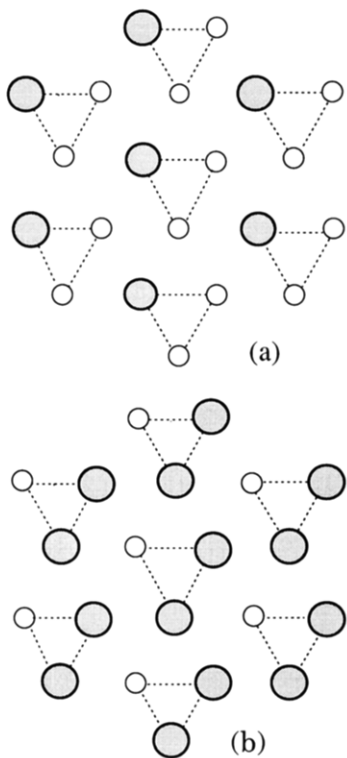


**Figure 7.** Corrugations in the surface sulfur atoms of an  $\text{MnPS}_3$  layer expected when the  $\text{P}_2\text{S}_6^{2-}$  ions tilt. The more protruded sulfur atoms are indicated by larger circles, and the three sulfur atoms belonging to a  $\text{PS}_3$  pyramid are joined by lines: (a)  $\theta > 0^\circ$  and (b)  $\theta < 0^\circ$ .

pattern. Within the experimental error of distance measurements,<sup>34</sup> the  $\sim 6.5 \text{ \AA}$  period of the superstructure is identical with the  $a$  parameter of the lattice ( $6.1 \text{ \AA}$ , Figure 1). As already pointed out, when every  $\text{P}_2\text{S}_6^{4-}$  ion is arranged with its P-P bond perpendicular to the  $\text{MnPS}_3$  layer (see 1), the surface sulfur atoms form a hexagonal lattice (Figure 1). Since each  $\text{P}_2\text{S}_6^{4-}$  ion is a covalently bonded unit, it is natural to consider its tilting motion as a rigid body. If the P-P bond of each  $\text{P}_2\text{S}_6^{4-}$  ion tilts as indicated in 2 (tilt angle  $\theta > 0^\circ$ ), one of the top three sulfur atoms of  $\text{P}_2\text{S}_6^{4-}$  becomes more protruded than the remaining two, thereby leading to the surface sulfur atom corrugation shown in Figure 7a, where the more protruded sulfur atoms form a superstructure of the  $\sim 6.5 \text{ \AA}$  period. For the tilting 3 of the  $\text{P}_2\text{S}_6^{4-}$  ions (tilt angle  $\theta < 0^\circ$ ), two of the top three sulfur atoms of  $\text{P}_2\text{S}_6^{4-}$  are more protruded than the remaining one, so that the more protruded surface sulfur atoms form a superstructure of the  $\sim 6.5 \text{ \AA}$  period shown in Figure 7b. For the tilt angles  $\theta = \pm 10^\circ$ , the surface sulfur atom corrugation has a height difference of  $\sim 0.5 \text{ \AA}$ .

An AFM image of a surface obtained with a contact mode is described by the total density plot of the surface,  $\varrho(r_0)$ . The latter is the surface electron density resulting from all the occupied energy levels (since all electrons are involved in the repulsive interactions with the tip) and evaluated at the tip-to-surface distance  $r_0$ . Recently, AFM images of numerous layered compounds<sup>39–41</sup>

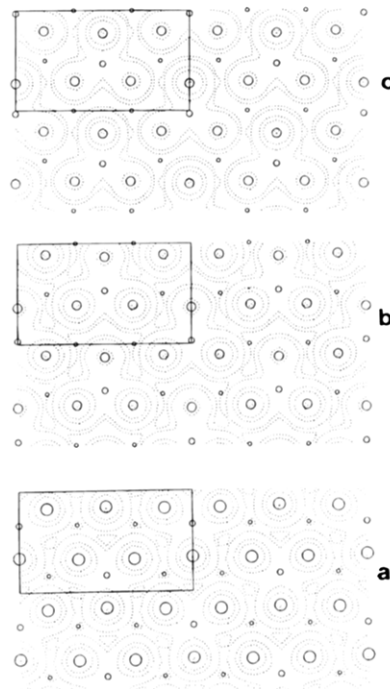


**Figure 8.** Total electron density plots  $\varrho(r_0)$  of an  $\text{MnPS}_3$  layer calculated for three different tilt angles of the  $\text{P}_2\text{S}_6^{2-}$  ions: (a)  $\theta = 0^\circ$ , (b)  $\theta = 10^\circ$ , and (c)  $\theta = -10^\circ$ . The surface sulfur atoms are represented by large circles, the phosphorus atoms by medium circles, and the Mn atoms by small circles. The plot area covers four unit cells, one of which is indicated by a rectangular box. The contour lines used are 0.2, 0.1, 0.05, 0.01, and 0.005 electrons/ $\text{au}^3$ . For our calculations,  $r_0$  was taken to be  $0.5 \text{ \AA}$  from the most protruded surface atoms, as in refs 37 and 38.

have been successfully analyzed on the basis of the  $\varrho(r_0)$  plots calculated by the extended Hückel tight-binding (EHTB) electronic band structure method.<sup>42</sup> In the present work, we calculate the electronic band structures of single  $\text{MnPS}_3$  layers with three different tilt angles  $\theta = +10^\circ$ ,  $0^\circ$ , and  $-10^\circ$  by employing the atomic parameters of the earlier study<sup>43</sup> and subsequently calculate the corresponding  $\varrho(r_0)$  plots (Figure 8). In these plots, density distributions are centered on the surface sulfur atoms, the more protruded sulfur atoms have a greater density, and the density patterns closely resemble the topography of the surface sulfur atoms. Therefore, the regular pattern is assigned to the surface sulfur atoms. The superstructure observed for  $\text{Mn}_{1-x}\text{PS}_3\text{G}_{2x}$  ( $\text{G} = \text{K}$ , pyH) is explained by the protruded sulfur atoms for a positive tilt angle  $\theta$ , and that for  $\text{Mn}_{1-x}\text{PS}_3(\text{Me}_4\text{N})_{2x}$  by the protruded sulfur atoms for a negative tilt angle  $\theta$ .

The tilting of the  $\text{P}_2\text{S}_6^{4-}$  ions in the topmost layers of the  $\text{Mn}_{1-x}\text{PS}_3\text{G}_{2x}$  ( $\text{G} = \text{K}$ , pyH,  $\text{Me}_4\text{N}$ ) intercalates may be caused most likely by the hydrated guest cations  $\text{G}^+$  (perhaps also some  $\text{Mn}^{2+}$ ) present between the adjacent

(39) (a) Magonov, S. N.; Zönnchen, P.; Rötter, H.; Thiele, G.; Cantow, H.-J.; Ren, J.; Whangbo, M.-H. *J. Am. Chem. Soc.* **1993**, *115*, 2495. (b) Whangbo, M.-H.; Ren, J.; Canadell, E.; Louder, D.; Parkinson, B.; Bengel, H.; Magonov, S. N. *J. Am. Chem. Soc.* **1993**, *115*, 3760. (c) Ren, J.; Whangbo, M.-H.; Bengel, H.; Magonov, S. N. *J. Phys. Chem.* **1993**, *97*, 4764. (d) Ren, J.; Whangbo, M.-H.; Bengel, H.; Cantow, H.-J.; Magonov, S. N. *Chem. Mater.* **1993**, *5*, 1018.

(40) (a) Bar, G.; Cantow, H.-J.; Magonov, S. N.; Kusch, N. D.; Yagubskii, E. B.; Paradis, J.; Ren, J.; Whangbo, M.-H. *New J. Chem.* **1993**, *17*, 439. (b) Magonov, S. N.; Bar, G.; Cantow, H.-J.; Paradis, J.; Whangbo, M.-H.; Yagubskii, E. B. *J. Phys. Chem.* **1993**, *97*, 9170. (c) Magonov, S. N.; Bar, G.; Cantow, H.-J.; Paradis, J.; Ren, J.; Whangbo, M.-H. *Synth. Met.* **1993**, *62*, 83. (d) Magonov, S. N.; Bar, G.; Cantow, H.-J.; Ren, J.; Whangbo, M.-H. *Synth. Met.*, in press.

(41) Parkinson, B. A.; Ren, J.; Whangbo, M.-H. *J. Am. Chem. Soc.* **1991**, *113*, 7833.

(42) Whangbo, M.-H.; Hoffmann, R. *J. Am. Chem. Soc.* **1978**, *100*, 6093.

(43) Whangbo, M.-H.; Brec, R.; Ouvrard, G.; Rouxel, J. *Inorg. Chem.* **1985**, *24*, 2459.

MnPS<sub>3</sub> layers and also possibly by the effect of Mn<sup>2+</sup> site vacancies. Then, what can be a cause for the superstructure image also observed for pure MnPS<sub>3</sub>? On the basis of the crystal structure of MnPS<sub>3</sub>, only the regular pattern of sulfur atoms is expected to be seen as in Figure 1a. We speculate that a tilting of the P<sub>2</sub>S<sub>6</sub><sup>4-</sup> ions in pure MnPS<sub>3</sub> can occur when water molecules from air are inserted between the top adjacent MnPS<sub>3</sub> layers of the sample. It is expected that the P<sub>2</sub>S<sub>6</sub><sup>4-</sup> ions of the topmost layer undergo a tilting motion to accommodate the guest species lying below, which is not difficult energetically because the Mn<sup>2+</sup> and P<sub>2</sub>S<sub>6</sub><sup>4-</sup> ions are not strongly bound as pointed out earlier.

### Concluding Remarks

Atomic-resolution AFM images of MnPS<sub>3</sub> and its intercalation compounds Mn<sub>1-x</sub>PS<sub>3</sub>G<sub>2x</sub> (G = K, pyH, Me<sub>4</sub>N) are characterized by two hexagonal patterns. The regular pattern of the ~3.5 Å period is explained by the surface sulfur atoms of the topmost layers, and the superstructure of the ~6.5 Å period by the protruded surface sulfur atoms that occur when the P<sub>2</sub>S<sub>6</sub><sup>4-</sup> ions tilt slightly from the perpendicular arrangement. The tilting of the P<sub>2</sub>S<sub>6</sub><sup>4-</sup> ions in the topmost layer may be caused by the guest species (e.g., Mn<sup>2+</sup> and G<sup>+</sup> ions or water molecules) lying below between the layers. Two slightly different superstructure patterns are generated depending on whether the tilt angle  $\theta$  is positive or negative. The superstructures of Mn<sub>1-x</sub>PS<sub>3</sub>G<sub>2x</sub> (G = K, pyH) are explained by  $\theta > 0^\circ$ , and those of Mn<sub>1-x</sub>PS<sub>3</sub>(Me<sub>4</sub>N)<sub>2x</sub> by  $\theta < 0^\circ$ . These "superstructures" due to the protruding S atoms do not imply any change in the *a* and *b* "in plane" parameters of the monoclinic unit cell of the host lattice. The *a* parameter is about 6.1 Å, which is equal to the separation between protruding S atoms. Therefore the present AFM results provide the first clear evidence for a "subtle" modification of the host lattice under the influence of intercalation. Only a refined X-ray structure determination of the intercalate could bring such information, but it is extremely difficult or impossible to get monocrystals of intercalates having sufficient quality to allow such a study.

Our results are consistent with the previous observations that intercalation of MPS<sub>3</sub> lowers the symmetry of the lattice<sup>27,30,31</sup> and allow us to suggest a structural model to explain our recent result<sup>27</sup> that the stilbazolium intercalates of MPS<sub>3</sub> possess strong spontaneous second-order NLO properties. The latter implies a noncentrosymmetrical arrangement of the chromophores and hence an alignment of their dipoles. Tilting the P<sub>2</sub>S<sub>6</sub><sup>4-</sup> ions obviously lowers the symmetry of the host lattice. The dipole moments of the PS<sub>3</sub> pyramids then become tilted all along the same direction, so that they add up along this specific direction. This process would generate an "internal" electric field in a specific direction in the close vicinity of the layer, which might be responsible for poling the dipolar chromophores. The electric field caused by tilting the P<sub>2</sub>S<sub>6</sub><sup>4-</sup> may be either reinforced or cancelled depending on how the adjacent slab is shifted and oriented with respect to the first one. However, AFM has an intrinsic limitation that it can give direct information only about the top layer. Further studies about the stacking mode are therefore

needed before we can suggest a precise model.

The high resolution of the images shown in this work might suggest that the imaging mechanism involves a lone atom at the end of the tip, which gently traces out the contours of the sample.<sup>44</sup> However, regarding the strong repulsive force applied ( $\approx 2.5 \times 10^{-8}$  N) and the contact mode employed to image the surface, a single atom tip would probably pierce the topmost slab.<sup>45,46</sup> It is therefore likely that a quite large contact area is involved in the imaging mechanism.<sup>47</sup> One possibility is that nanoflakes of the top layer are broken off by the tip and dragged along the next layer, as suggested in the Pethica's sliding contact model of graphite imaging.<sup>48</sup> Therefore, it cannot be definitely ruled out that the superlattice images could arise from the imaging mechanism itself. It is worthwhile recalling here that no general theory of the imaging mechanism in AFM is available at present.<sup>49</sup> Nevertheless, we have some reasons to believe that the images obtained in this work describe actual features of the materials, whatever the mechanism may be. Thus, the images of the top layer of pure MnPS<sub>3</sub> (such as Figure 2a) perfectly reproduce the pattern expected from the already known crystallographic structure (hexagonal array of sulfur atoms 3.5 Å apart). In contrast, scanning a Mn<sub>1-x</sub>PS<sub>3</sub>K<sub>2x</sub> intercalate always gives the image shown in Figure 5 with the superstructure and never gives an image such as Figure 2a. Therefore, this is a difference that goes along with the chemical change carried out (intercalation) and that is highly reproducible. In addition, the images obtained are reasonably consistent with the body of results already known regarding the structural, physical, and chemical properties of these compounds (X-ray evidence for superstructure, occurrence of intralayer vacancies which obviously can be a source for distortions, lowering of symmetry associated with intercalation, as described above). Therefore, we are confident that the various images described in this work provide direct evidence on the atomic scale for genuine modifications that actually occur in the compounds. We even think that the the possibility offered by intercalation chemistry to image a material that can be modified in a controlled manner can help theoreticians to design new models for imaging mechanisms in AFM.

**Acknowledgment.** Work at Université de Paris-Sud was supported by the MRES, the CNRS (Ultimatech) and the Conseil General de l'Essonne, and at North Carolina State University by the Office of Basic Energy Sciences, Division of Materials Sciences, U.S. Department of Energy, under Grant DE-FG05-86ER45259. We also thank Dr. Poulin and Dr. Paris (Instrumat) for their kind help.

(44) Burnham, N. A.; Colton, R. J. In *Scanning Tunneling Microscopy and Spectroscopy: Theory, Techniques and Applications*; Bonnell, D. A., Ed.; VCH Publishers: New York, 1993; pp 191–249.

(45) Abraham, F. F.; Batra, I. P. *Surf. Sci. Lett.* **1989**, *209*, L125.

(46) Heinzemann, H.; Meyer, E.; Brodeck, D.; Overney, G.; Güntherodt, H.-J. *Z. Phys. B, Condensed Matter* **1992**, *88*, 321.

(47) Mizes, H. A.; Park, S.-I.; Harrison, W. A. *Phys. Rev. B* **1987**, *36*, 4491.

(48) Pethica, J. B. *Phys. Rev. Lett.* **1986**, *57*, 3235.

(49) Overney, G.; Zhong, W.; Tomanek, D. *J. Vac. Sci. Technol. B* **1991**, *9*, 479.